





Nonlinear scaling in photon momentum transfer caused by two-electron effectsYong-Kang Fang ¹, Hao Liang ¹, Wei-Chao Jiang ^{2,*} and Liang-You Peng ^{1,3,4,5,†}¹*State Key Laboratory for Mesoscopic Physics and Frontiers Science Center for Nano-optoelectronics, School of Physics, Peking University, Beijing 100871, China*²*College of Physics and Optoelectronic Engineering, Shenzhen University, Shenzhen 518060, China*³*Collaborative Innovation Center of Quantum Matter, Beijing 100871, China*⁴*Collaborative Innovation Center of Extreme Optics, Shanxi University, 030006 Taiyuan, China*⁵*Peking University Yangtze Delta Institute of Optoelectronics, Nantong, Jiangsu 226010, China*

(Received 26 January 2022; revised 14 June 2022; accepted 25 July 2022; published 8 August 2022)

The photon momentum transfer in the two-photon double ionization of helium is theoretically studied based on the *ab initio* calculations. A nonlinear dependence of the transferred momentum on the photon energy is identified at relatively small photon energies. As expected, the linear dependence is recovered with the slope approaching 1.60 when the photon energy becomes sufficiently large. With a semianalytical model including the Coulomb screen effect in the two-electron ground state, we can qualitatively reproduce the nonlinear dependence and find that it is mainly contributed by the fast electron. However, compared with the results from the *ab initio* calculations, the quantitative discrepancies at relatively small photon energies can be accounted for only by the electron correlation in the intermediate state. The present study reveals the vital roles played by the two-electron effects for the complicated photon momentum transfer process in the few-photon and few-electron systems.

DOI: [10.1103/PhysRevA.106.023104](https://doi.org/10.1103/PhysRevA.106.023104)**I. INTRODUCTION**

In the theoretical studies of ionization dynamics, the dipole approximation is usually employed, in which the laser pulse is assumed to be independent on space coordinates. However, this approximation will break down when the wavelength is short enough to be comparable with the atom size or when the laser field is so intense that the magnetic field effects cannot be neglected [1]. The photon momentum transfer in the ionization process is one of the prominent nondipole effects, which is related to the unsymmetrical photoelectron distribution with respect to the propagation direction of the pulse [2].

In 2011 it was experimentally determined that the photon momentum transferred to the photoelectron, in the single ionization of atoms by intense 800 and 1400 nm circularly polarized laser pulses [3], almost equals the average energy of photoelectron divided by the speed of light. Later the shift of photoelectron momentum spectra to the opposite direction of the laser propagation was identified with linearly polarized laser pulses [4]. Meantime, a large number of theoretical studies have been carried out [5–11]. In particular, Chelkowski *et al.* found that the residual ion carries only part of the momentum corresponding to the ionization potential [8], which was confirmed in a recent experiment [12].

In fact, the study of the photon momentum transfer in the high-frequency weak-field regime has a much longer history. Even in the early stage of quantum mechanics, Sommerfeld *et al.* had shown that the photon can transfer a larger momen-

tum to the electron than it carries [13]. The momentum-energy scaling law has been derived for different initial states of the hydrogen-like atoms [14,15]. Recently, theoretical studies were extended to the two- and three-photon ionization of the hydrogen-like atom [10,16] and to the one-photon single ionization (PSI) of a diatomic molecule [17,18]. Benefiting from the rapid development of the bright light sources from the high-order harmonic generation [19,20] and the free-electron lasers [21–23], the experimental measurements for the momentum transfer in high-frequency regime gradually have become possible [24].

As a two-electron atom, helium provides an ideal platform to study the electron correlation, which allows quantitative comparisons of differential observables from theory and experiment. One of recent examples is the photon momentum transfer in the one-photon double ionization (PDI) [25], for which a joint theoretical and experimental study reveals the partition laws of the photon momentum among the three particles. However, things will be much more complicated and different in the regime of two-photon double ionization (TPDI) of helium, which is the simplest case of the few-photon and few-electron system where the photon momentum transfer has not yet been explored. In particular, at relatively low photon energies in the nonsequential and sequential regime, it is crucial to investigate how the two-electron effects including the electron correlation will change the partition laws in the photon momentum transfer and alter the coefficients in the momentum-energy scaling.

In this work, we systematically study the photon momentum transfer in TPDI by solving the full-dimensional time-dependent Schrödinger equation (TDSE). We find that the photon momentum transfer is strongly affected by the

*jiang.wei.chao@szu.edu.cn

†liangyou.peng@pku.edu.cn

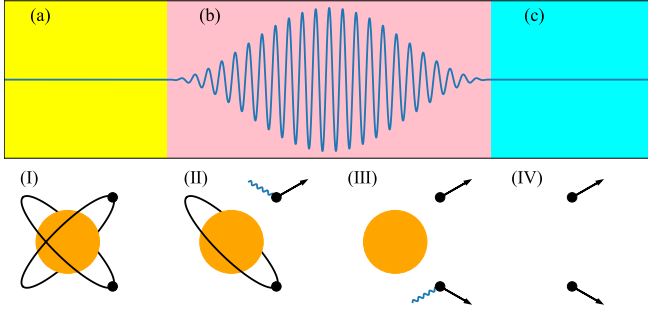


FIG. 1. Illustration of the four steps of TPDI of helium. The electron correlation in TPDI can be divided into three types, i.e., in the initial state (a, I), in the intermediate state (b, II, III), and in the final state (c, IV).

two-electron effect, which results in a nonlinear increase of the coefficient of the momentum-energy scaling law. The expected value of 1.60 for the PSI of the ground state of the hydrogen-like atom is found in the asymptotic regime at large photon energies. Based on the virtual sequential picture [26] including the Coulomb screen effect in the initial state, we develop a semianalytical model that can qualitatively reproduce our findings, while the electron correlation in the intermediate state is needed to quantitatively reproduce the scaling law in the relatively low photon energy regime.

The rest of this paper is organized as follows. In Sec. II we give a brief introduction of our TDSE method and the semianalytical model based on the virtual sequential picture. In Sec. III we present our results about the momentum transfer in the TPDI of helium. Detailed analysis is given to show the importance of the two-electron effect. In Sec. IV we give a brief summary. Unless otherwise stated, atomic units are used throughout this work.

II. THEORETICAL METHODS

The process of TPDI of helium can be illustrated by the four steps shown in Fig. 1. Due to the long-range nature of the Coulomb potential, different vital roles may be played by the electron correlation in each step, depending on the photon energy and the duration of the applied laser pulse. Usually, the electron correlation can be referred to the initial state, the intermediate state, and the final state correlation. For the sequential TPDI with a relatively long laser pulse, the electron correlation in the intermediate state and the final state is of less importance. However, in the nonsequential regime or for a very short pulse, the electron correlation in these two stages will be important [27].

Our calculations are mainly based on the numerical solution to the full-dimensional TDSE beyond the dipole approximation [25]. The interaction Hamiltonian can be written either in the length gauge (LG) or in the velocity gauge (VG) [25]. Details of our TDSE method can be found in our previous paper [28]. Here we give only a brief introduction of the method and specify the parameters used in this study. In the spherical coordinates, we employ the finite element discrete variable representation (FE-DVR) [29,30] method to discretize the radial coordinates and the Lanczos propagator

to evolve the two-electron wave. The maximal numbers of the single angular momentum (l_{\max}) and total angular momentum (L_{\max}) are set to be 5 and 4, respectively. The average radial spacing is about 0.25 a.u. After the end of the pulse, the wave function is further propagated for 40 a.u. so that one can project it to the product of two Coulomb waves and obtain the differential momentum distribution of the two electrons $P(\mathbf{k}_1, \mathbf{k}_2)$, from which all other physical observables can be computed. The calculations are made for circularly polarized laser pulses, propagating along z axis, with a wide range of photon energies from 42 to 150 eV, but at a fixed peak intensity of 10^{12} W/cm² with the \sin^2 envelope. The pulse duration is set to be 2 fs from 42 to 70 eV and 20 cycles from 70 to 150 eV, respectively. The propagation time step is 0.01 a.u. Convergence of our results has been ensured against the change of all spatial and temporal parameters.

To get the physical insights of the TDSE results, we turn to the second-order time-dependent perturbation theory (TDPT) based on the virtual sequential picture. Previously, it has been used to study the total ionization probability and energy differential spectrum in both the sequential TPDI regime and the nonsequential TPDI regime [26,31–36]. According to the model, the momentum distribution of the two electrons is given by

$$P_{\text{model}}(\mathbf{k}_1, \mathbf{k}_2) = \int d\mathbf{k} \int_{t_i}^{t_f} dt_2 e^{i(E_f - E_s)t_2} \langle f | H_I(t_2) | s, \mathbf{k} \rangle \times \int_{t_i}^{t_2} dt_1 e^{i(E_s - E_i)t_1} \langle s, \mathbf{k} | H_I(t_1) | i \rangle, \quad (1)$$

in which $|i\rangle$ is the ground state of the helium and can be calculated with the method of imaginary time propagation of the two-electron TDSE, $|s, \mathbf{k}\rangle$ is the intermediate state which is approximated by the symmetric product of the Coulomb wave and the ground state of He^+ , and $|f\rangle$ is the symmetric product of two Coulomb waves. In the velocity gauge, the interaction Hamiltonian H_I is given by

$$H_I(t) = \sum_{j=1,2} \{-i\mathbf{A}(t) \cdot \nabla_j - i\alpha(\hat{\mathbf{k}}_\gamma \cdot \mathbf{r}_j)[\mathbf{E}(t) \cdot \nabla_j] + \alpha(\hat{\mathbf{k}}_\gamma \cdot \mathbf{r}_j)[\mathbf{A}(t) \cdot \mathbf{E}(t)]\}, \quad (2)$$

with α , $\hat{\mathbf{k}}_\gamma$, $\mathbf{A}(t)$, and $\mathbf{E}(t)$ being the fine-structure constant, the propagation direction of laser pulse, the vector potential, and the electric field, respectively. All the Coulomb waves are evaluated with the nuclear charge number of 2. As can be noticed, part of the electron correlation in the initial state has been taken into account by taking the exact ground state of helium under the consideration of only one prominent partial wave with $l_1 = l_2 = L = M = 0$, while the electron correlation in the intermediate and final state is neglected.

Also, one can construct the initial state based on the Hartree-Fock method, which is regarded as the noncorrelated wave function. The two-electron effect is limited to the mean-field correlation, which can be regarded as the Coulomb screen effect. The corresponding results in Sec. III are the same as the partly correlated initial state, which suggests the initial state electron correlation behaves as the Coulomb screen effect here. Therefore, we will call it the Coulomb screen effect hereafter.

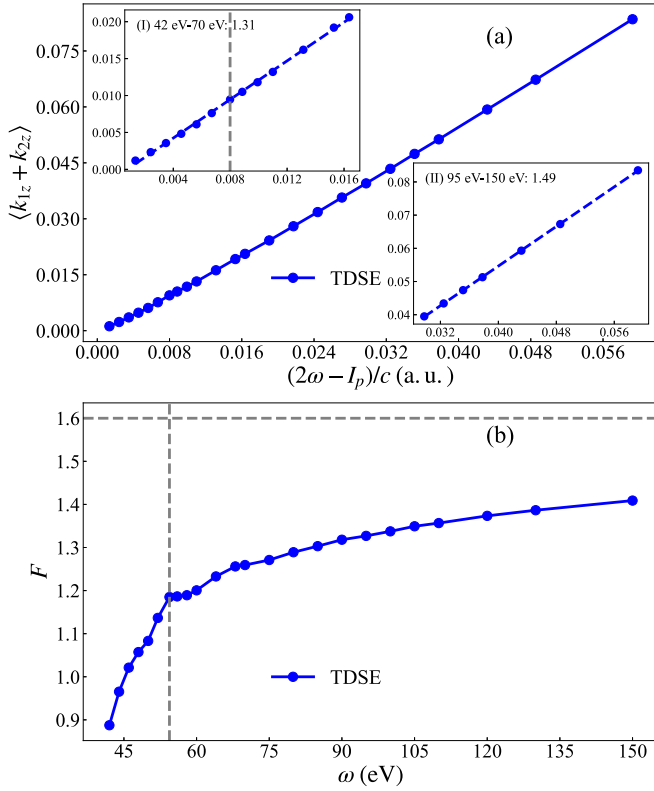


FIG. 2. (a) The sum of the momenta transferred to the two photoelectrons for laser pulses with $\omega \in (42, 150)$ eV. Insets I and II show a linear fitting in different ranges with the slope being 1.31 and 1.49, respectively. (b) F (see text for definition) as a function of the photon energy. The horizontal gray dashed line represents the asymptotic value of 1.60, corresponding to that for PSI of the ground state of hydrogen-like atom. The vertical gray dashed line marks the boundary of the sequential and the nonsequential regimes.

Please note that we numerically calculate the transition matrix elements instead of using the value of a one-photon single-ionization cross section [37], which means that the phase information is preserved in our model. Details of the TDPT model can be found in Appendix A.

III. RESULTS

The main physical quantities we concern in this work are the averaged momenta of the two photoelectrons in the propagation direction of laser pulse, whose sum can be evaluated by

$$\langle k_{z1} + k_{z2} \rangle = \iint d\mathbf{k}_1 d\mathbf{k}_2 (k_{z1} + k_{z2}) \tilde{P}(\mathbf{k}_1, \mathbf{k}_2), \quad (3)$$

where $\tilde{P}(\mathbf{k}_1, \mathbf{k}_2) = P(\mathbf{k}_1, \mathbf{k}_2)/P_{\text{total}}$ with $P_{\text{total}} = \iint d\mathbf{k}_1 d\mathbf{k}_2 P(\mathbf{k}_1, \mathbf{k}_2)$. In Fig. 2(a) we show the results of $\langle k_{z1} + k_{z2} \rangle$ as a function of E_{ex}/c where the excess energy $E_{\text{ex}} = 2\omega - I_p$ with I_p being the double ionization potential of helium. As expected, one finds that the total momentum $\langle k_{z1} + k_{z2} \rangle$ is always a positive value regardless of the photon energy. A striking feature is the nonlinear scaling at relatively smaller photon energies, which can be confirmed by a linear fitting in different regions of photon energies, as shown in insets I and II of Fig. 2(a). The slope of the

linear fitting is 1.31 and 1.49, respectively. A better way to show the nonlinear dependence is to define a parameter $F = \langle k_{1z} + k_{2z} \rangle / [(2\omega - I_p)/c]$, whose value is shown in Fig. 2(b) as a function of the photon energy ω . It is clearly seen that F gradually increases and will eventually approach the well-known value of 1.60, as will be seen below.

Using $P(\mathbf{k}_1, \mathbf{k}_2)$ from TDSE or $P_{\text{model}}(\mathbf{k}_1, \mathbf{k}_2)$ from the model, one can calculate the momentum of the fast and the slow electron in the propagation direction

$$\begin{aligned} \langle k_{\text{fast}} \rangle &= 2 \iint d\mathbf{k}_1 d\mathbf{k}_2 k_{z1} \eta(k_1 - k_2) \tilde{P}(\mathbf{k}_1, \mathbf{k}_2), \\ \langle k_{\text{slow}} \rangle &= 2 \iint d\mathbf{k}_1 d\mathbf{k}_2 k_{z1} \eta(k_2 - k_1) \tilde{P}(\mathbf{k}_1, \mathbf{k}_2), \end{aligned} \quad (4)$$

where η is the Heaviside step function. Let us first consider the photon energy range of (95, 150) eV, in which the virtual sequential model is expected to work better in the sequential regime. In the left column of Fig. 3, we show the results from both the TDSE and the model. As one can see, very good agreements are achieved for both the total momentum and the individual momentum of each electron along the laser propagation direction. Thus, in the sequential regime, one can indeed regard the TPDI as a two-step process, i.e., the PSI of helium and the subsequent PSI of the ground state of He^+ (with the neglect of the shake-off mechanism [35,38]). The current result for the photon momentum transfer is consistent with previous studies [31,32,35]. Therefore, after neglecting the small intercept term, the momentum-energy scaling law in the photon momentum transfer can be given by

$$\begin{aligned} \langle k_{\text{fast}} \rangle &= \alpha_f (\omega - I_{p1}), \quad \langle k_{\text{slow}} \rangle = \alpha_s (\omega - I_{p2}), \\ \langle k_{\text{total}} \rangle &= \frac{\alpha_f + \alpha_s}{2} (2\omega - I_p) + \frac{\alpha_f - \alpha_s}{2} (I_{p2} - I_{p1}), \end{aligned} \quad (5)$$

where I_{p1} and I_{p2} are the single ionization potential of He and He^+ , respectively.

Provided with these excellent agreement in the sequential regime, one can extend the results of the TDPT model in a range of large photon energies, i.e., (800, 1000) eV, in which region TDSE calculations are formidable due to the extremely large computational resources. As shown in the right column of Fig. 3, one finds that the slope indeed approaches the expected value of 1.60 for the hydrogen-like atom [Fig. 3(b)]. A prominent feature from Figs. 3(c) and 3(d) is that the slope of the slow electron is always close to 0.80. This good linear dependence of the slow (the second) electron means that the nonlinear dependence of the momentum-energy scaling law of the TPDI mainly comes from the first PSI of helium α_f [cf. Eq. (5)]. Based on the nice agreement between results of TDSE and the model and the fact that the Coulomb screen effect in the initial state is included in our model, one can infer that the nonlinear dependence in the momentum-energy scaling law mainly originates from the Coulomb screen effect in the initial state.

The nonlinear dependence induced by the Coulomb screen effect of the first (the fast) electron can be understood as follows. For the single-electron atom case, it was found that the momentum-energy scaling law is dominated by the short-range property of the potential in the ground state [16]. It is known that the ionized electron momentum distribution is

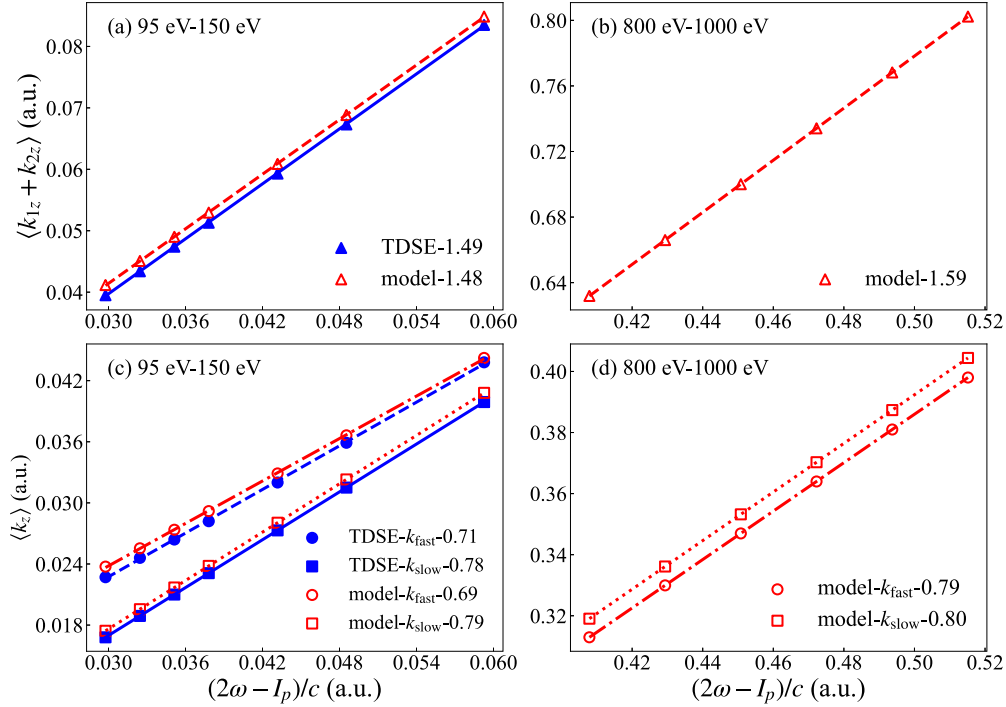


FIG. 3. The sum of the momenta transferred to the two photoelectrons and the respective momentum of each electron at different photon energy range marked in each panel. The lines in each panel represent a linear fitting of the results from either the TDSE or the TDPT model, and their slopes are indicated in the legend.

closely related to the Fourier transform of the initial state in the real space [8]. Thus, for a single electron atom, a higher electron energy (thus a corresponding higher photon energy) will be related to the behavior of the shorter range of the atomic potential where the cusp of the electron and the nucleus exists. For the two-electron system, the behavior of the extremely short range of the potential is still dominated by the Coulomb potential between one electron and the nucleus. However, with the intermediate photon energies of tens of electron volts, the corresponding range in the real space will be influenced by the cusp between the two electrons [39–44] (equivalently, the Coulomb screen effect from the two-electron effect), which results in the change of the coefficient in the momentum-energy scaling law. In this spirit, the nonlinear behavior can also be qualitatively reproduced by the calculations of PSI of helium with a single-active-electron (SAE) model potential with $V_{\text{eff}} = -\frac{1}{r}[1 + (1 + \frac{27}{16}r)e^{-\frac{27}{8}r}]$ (for clarity, the results are shown in Appendix B). We find that, although the SAE approximation works rather well in the high-energy regime, there exist significant discrepancies from results of the two-electron TDSE at lower photon energies, which may be attributed to the electron correlation in the intermediate state. In addition, due to the nonlinear dependence of the α_f , the slower electron will carry a larger momentum in the direction of laser pulse at extremely large photon energies, which is shown in Fig. 3(d).

We now turn to the nonsequential and sequential regime of the TPDI at smaller photon energies, where calculations from both the TDSE and the TDPT model have been carried out. In this region, we plot the momentum-energy scaling law against the excess energy. One can compute the excess energy of the

fast and the slow electron, respectively, by

$$\begin{aligned} \langle E_{\text{fast}} \rangle &= 2 \iint d\mathbf{k}_1 d\mathbf{k}_2 E_1 \eta(k_1 - k_2) \tilde{P}(\mathbf{k}_1, \mathbf{k}_2), \\ \langle E_{\text{slow}} \rangle &= 2 \iint d\mathbf{k}_1 d\mathbf{k}_2 E_1 \eta(k_2 - k_1) \tilde{P}(\mathbf{k}_1, \mathbf{k}_2), \end{aligned} \quad (6)$$

with $E_1 = k_1^2/2$ whose definitions are suitable for both the nonsequential and the sequential regime. In the sequential regime for a relatively long pulse, one can numerically check that these two formulas indeed reduce to $\langle E_{\text{fast}} \rangle \approx \omega - I_{p1}$ and $\langle E_{\text{slow}} \rangle \approx \omega - I_{p2}$ respectively. The total excess energy is always given by $\langle E_{\text{exc}} \rangle \approx 2\omega - I_p$. With these, one can rewrite the momentum-energy scaling law for the fast and the slow electron in Eq. (5) as

$$\langle k_{\text{fast}} \rangle = \beta_f \langle E_{\text{fast}} \rangle, \quad \langle k_{\text{slow}} \rangle = \beta_s \langle E_{\text{slow}} \rangle. \quad (7)$$

As can be seen from Fig. 4(a), it is interesting to note that the global behavior of the fast electron and the slow electron can still be well described by the model, although the electron correlation in the intermediate state for the nonsequential TPDI regime is neglected. What is more, one finds the momentum-energy scaling law for the fast electron is almost the same from the nonsequential to the sequential regime of the TPDI, as shown in Fig. 4(b). However, if the linear fitting of the fast electron is done in the regimes of 42–50 eV and 58–70 eV, respectively, the slope will be 1.29, 1.27 for the TDPT model and 1.17, 1.21 for the TDSE. The model loses the ability to well reproduce the TDSE results, which is attributed to the neglecting of the electron correlation in the intermediate state. This is confirmed by the results of TDSE propagation with the Hartree-Fock initial state, which can be

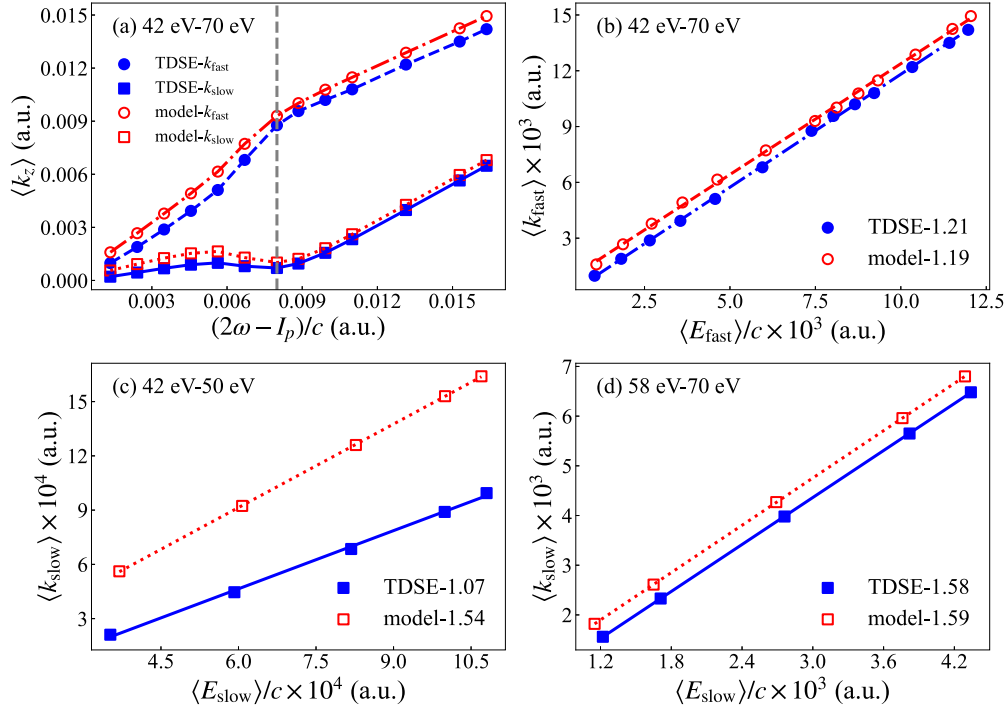


FIG. 4. The total and respective photon momentum transferred at relatively lower photon energies of $\omega \in (42, 70)$ eV. The gray dashed line in (a) marks the boundary of the nonsequential and the sequential regimes. In (b), (c), and (d), the photon momentum transferred for the fast or the slow electron is linearly fitted in different ranges of its average energy divided by c , with the slope indicated in the legend.

seen in Table I. For the slow electron, the TDPT model fails to describe the scaling law in the nonsequential regime but successfully predicts it in the sequential regime, as shown in Figs. 4(c) and 4(d). The difference also comes from the electron correlation in the intermediate state.

One notices that the momentum-energy scaling law in the sequential TPD1 at smaller photon energies is consistent with that at large photon energies discussed previously. However, according to Eq. (7), the scaling law in the nonsequential regime should be given by

$$\begin{aligned} \langle k_{\text{total}} \rangle &= \beta_f \langle E_{\text{fast}} \rangle + \beta_s \langle E_{\text{slow}} \rangle \\ &= \left[\frac{\beta_f + \beta_s}{2} + \frac{\beta_f - \beta_s}{2} \frac{\langle E_{\text{diff}} \rangle}{\langle E_{\text{total}} \rangle} \right] \langle E_{\text{total}} \rangle, \end{aligned} \quad (8)$$

where $\langle E_{\text{diff}} \rangle = \langle E_{\text{fast}} \rangle - \langle E_{\text{slow}} \rangle$ and $\langle E_{\text{total}} \rangle = \langle E_{\text{fast}} \rangle + \langle E_{\text{slow}} \rangle$. According to the numerical results in Figs. 4(b) and 4(c), one gets $\beta_f \approx 1.20$ and $\beta_s \approx 1.10$, which means that the total coefficient approximately equals the average of β_f and

β_s . This can be confirmed by the TDSE results in the photon energy range of [42, 50] eV. From the above discussions, in the relatively low photon energy regime, the Coulomb screen effect in the initial state and electron correlation in the intermediate state both play important roles. Finally, we mention that it is appropriate to neglect the electron correlation in the final state, which is confirmed by projection with different free-propagation time.

IV. SUMMARY

In summary, the photon momentum transfer in the two-photon double ionization of helium is theoretically studied by solving the full dimensional TDSE and by a virtual sequential TDPT model in a wide range of photon energies. We find that the coefficient of momentum-energy scaling law related to the photon momentum transfer increases nonlinearly with the photon energy and ultimately approaches the expected value of 1.60 for the PSI of the ground state of a hydrogen-like atom.

TABLE I. Results of TDSE propagation with fully correlated ground state (FC) or Hartree-Fock ground state (HF).

ω (eV)	$\langle k_{\text{fast}} \rangle^a$		$\langle E_{\text{fast}} \rangle^b$		$\langle k_{\text{slow}} \rangle^a$		$\langle E_{\text{slow}} \rangle^b$	
	FC	HF	FC	HF	FC	HF	FC	HF
42	0.979	0.979	14.24	14.24	0.211	0.211	4.829	4.829
46	2.878	2.878	36.38	36.38	0.685	0.685	11.21	11.21
54.4	8.770	8.770	101.2	101.2	0.703	0.703	9.505	9.505
68	13.50	13.50	156.5	156.5	5.653	5.653	52.33	52.33

^aAverage momentum is given in 10^{-3} a.u.

^bAverage energy is given in 10^{-2} a.u.

More detailed studies reveal that the Coulomb screen effect in the initial state plays a vital role in the nonlinear momentum-energy scaling law. In particular, in order to quantitatively evaluate the coefficient of the momentum-energy scaling law, one needs to consider the intermediate state electron correlation. The present study represents an important step to explore the photon momentum transfer in the few-photon and few-electron systems, which will trigger possible experimental investigations in the near future.

ACKNOWLEDGMENTS

This work is supported by National Natural Science Foundation of China Grants No. 11725416, No. 11961131008, and No. 12074265 and by National Key R&D Program of China Grant No. 2018YFA0306302.

APPENDIX A: DETAILS OF THE TDPT MODEL

In this Appendix, we show the details of the TDPT model of a helium atom beyond dipole approximation. The laser propagation direction is set to be the z axis.

1. The transition matrix elements of a single-electron atom

Before we show the TDPT model for the TPDI of a helium atom, we show the transition matrix elements for the PSI of a single-electron atom. For a single-electron atom interacting with the laser field, in the velocity gauge, the Hamiltonian is given by

$$\begin{aligned} H &= H_0 - i\mathbf{A}(t) \cdot \nabla + \alpha(\hat{\mathbf{k}}_\gamma \cdot \mathbf{r})[A(t) \cdot \mathbf{E}(t)] \\ &\quad - i\alpha(\hat{\mathbf{k}}_\gamma \cdot \mathbf{r})[\mathbf{E}(t) \cdot \nabla] \\ &= H_0 + D + H_a + H_b, \end{aligned} \quad (\text{A1})$$

with H_0 , D , H_a , and H_b being the field-free Hamiltonian, dipole term, and two nondipole terms, respectively. We suppose that the initial state $|i\rangle$ is s state and the final state $|\mathbf{k}\rangle$ can be represented by the Coulomb wave. Then the expression of the initial state and final state can be written by

$$\begin{aligned} |i\rangle &= R(r)Y_0^0(\hat{\mathbf{r}}), \\ |\mathbf{k}\rangle &= \frac{1}{\sqrt{2\pi k}} \sum_{l,m} i^l e^{-i(\sigma_l + \delta_l)} [Y_l^m(\hat{\mathbf{k}})]^* \tilde{R}_{k,l}(r) Y_l^m(\hat{\mathbf{r}}). \end{aligned} \quad (\text{A2})$$

Then the transition matrix elements can be given by

$$\begin{aligned} \langle \mathbf{k} | D | i \rangle &= D(k) A_x [Y_1^{-1}(\hat{\mathbf{k}}) - Y_1^1(\hat{\mathbf{k}})] \\ &\quad + D(k) i A_y [Y_1^{-1}(\hat{\mathbf{k}}) + Y_1^1(\hat{\mathbf{k}})], \\ \langle \mathbf{k} | H_a | i \rangle &= A(k) (A_x E_x + A_y E_y) Y_1^0(\hat{\mathbf{k}}), \\ \langle \mathbf{k} | H_b | i \rangle &= B(k) E_x [Y_2^{-1}(\hat{\mathbf{k}}) - Y_2^1(\hat{\mathbf{k}})] \\ &\quad + B(k) i E_y [Y_2^{-1}(\hat{\mathbf{k}}) + Y_2^1(\hat{\mathbf{k}})], \end{aligned} \quad (\text{A3})$$

where the definition of the parameters $D(k)$, $A(k)$, and $B(k)$ can be written by

$$\begin{aligned} D(k) &= -\frac{1}{\sqrt{12\pi k}} e^{i(\sigma_1 + \delta_1)} \\ &\quad \times \int dr [r \tilde{R}_{k,1}(r)] \left(\frac{\partial}{\partial r} - \frac{1}{r} \right) [rR(r)], \\ A(k) &= (-i)\alpha \frac{1}{\sqrt{6\pi k}} e^{i(\sigma_1 + \delta_1)} \\ &\quad \times \int dr [r \tilde{R}_{k,1}(r)] r [rR(r)], \\ B(k) &= (-i)^3 \alpha \frac{1}{\sqrt{60\pi k}} e^{i(\sigma_2 + \delta_2)} \\ &\quad \times \int dr [r \tilde{R}_{k,2}(r)] \left[r \frac{\partial}{\partial r} - 1 \right] [rR(r)]. \end{aligned} \quad (\text{A4})$$

2. The transition matrix elements of the TDPT model

As described in Sec. II, the expressions of the momentum distribution of the two electrons in the TDPT model $P_{\text{model}}(\mathbf{k}_1, \mathbf{k}_2)$ and the interaction Hamiltonian H_I are given in Eqs. (1) and (2), respectively.

In the TDPT model, the initial state $|i\rangle$, the intermediate state $|s, \mathbf{k}\rangle$, and the final state $|f\rangle$ can be given by

$$\begin{aligned} |i\rangle &= \frac{R(r_1, r_2)}{r_1, r_2} Y_0^0(\Omega_1) Y_0^0(\Omega_2), \\ |s, \mathbf{k}\rangle &= \frac{1}{\sqrt{2}} [|\mathbf{k}(r_1)\rangle |s(r_2)\rangle + |\mathbf{k}(r_2)\rangle |s(r_1)\rangle], \\ |f\rangle &= \frac{1}{\sqrt{2}} [|\mathbf{k}_1(r_1)\rangle |\mathbf{k}_2(r_2)\rangle + |\mathbf{k}_1(r_2)\rangle |\mathbf{k}_2(r_1)\rangle], \end{aligned} \quad (\text{A5})$$

with $|s\rangle = R_{\text{He}^+}(r) Y_0^0(\hat{\mathbf{r}})$. Therefore, taking the symmetry of two electrons into consideration, the two matrix elements in Eq. (1) can be given by

$$\begin{aligned} \langle s, \mathbf{k} | H_I | i \rangle &= \sqrt{2} \langle \mathbf{k}(r_1) s(r_2) | H_I(r_1) | i \rangle, \\ \langle f | H_I | s, \mathbf{k} \rangle &= \langle \mathbf{k}_1(r) | H_I(r) | s(r) \rangle \delta_{\mathbf{k}_2, \mathbf{k}} \\ &\quad + \langle \mathbf{k}_2(r) | H_I(r) | s(r) \rangle \delta_{\mathbf{k}_1, \mathbf{k}}. \end{aligned} \quad (\text{A6})$$

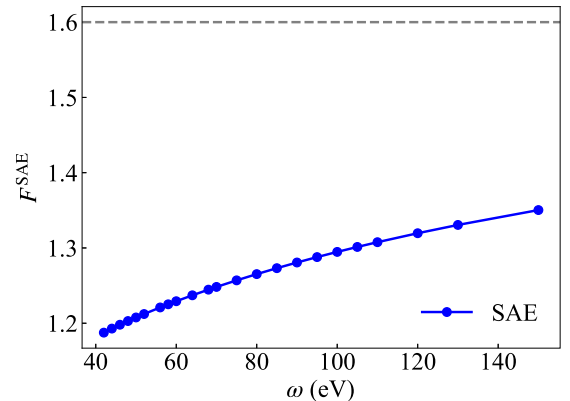


FIG. 5. The parameter F^{SAE} as a function of the photon energy.

One finds that in order to calculate the two-electron momentum distribution, we need only to know the transition matrix elements for single electron, which has already been given. In past studies based on the virtual sequential picture [26,31–36], dipole approximation is used, and the transition matrix

elements in Eq. (A6) can be related to the cross section [37]. However, in order to consider the nondipole effect, we need to calculate the transition matrix elements numerically.

According to the discussion above, the transition matrix elements of the TDPT model can be given by

$$\begin{aligned}
 \langle s, \mathbf{k} | H_I | i \rangle &= \Pi_1^1(k) A_x [Y_1^{-1}(\hat{\mathbf{k}}) - Y_1^1(\hat{\mathbf{k}})] + \Pi_1^1(k) i A_y [Y_1^{-1}(\hat{\mathbf{k}}) + Y_1^1(\hat{\mathbf{k}})] + \Pi_2^1(k) E_x [Y_2^{-1}(\hat{\mathbf{k}}) - Y_2^1(\hat{\mathbf{k}})] \\
 &\quad + \Pi_2^1(k) i E_y [Y_2^{-1}(\hat{\mathbf{k}}) + Y_2^1(\hat{\mathbf{k}})] + \Pi_{10}^1(A_x E_x + A_y E_y) Y_1^0(\hat{\mathbf{k}}) \\
 &= \sum_{l,m} (-m) \Pi_l^1 (F_l^x - m i F_l^y) Y_l^m(\hat{\mathbf{k}}) + \Pi_{10}^1 (F_1^x F_2^x + F_1^y F_2^y) Y_1^0(\hat{\mathbf{k}}) \quad (l = 1, 2; m = 1, -1), \\
 \langle \mathbf{k} | H_I | s \rangle &= \Pi_1^2(k) A_x [Y_1^{-1}(\hat{\mathbf{k}}) - Y_1^1(\hat{\mathbf{k}})] + \Pi_1^2(k) i A_y [Y_1^{-1}(\hat{\mathbf{k}}) + Y_1^1(\hat{\mathbf{k}})] + \Pi_2^2(k) E_x [Y_2^{-1}(\hat{\mathbf{k}}) - Y_2^1(\hat{\mathbf{k}})] \\
 &\quad + \Pi_2^2(k) i E_y [Y_2^{-1}(\hat{\mathbf{k}}) + Y_2^1(\hat{\mathbf{k}})] + \Pi_{10}^2(A_x E_x + A_y E_y) Y_1^0(\hat{\mathbf{k}}) \\
 &= \sum_{l,m} (-m) \Pi_l^2 (F_l^x - m i F_l^y) Y_l^m(\hat{\mathbf{k}}) + \Pi_{10}^2 (F_1^x F_2^x + F_1^y F_2^y) Y_1^0(\hat{\mathbf{k}}) \quad (l = 1, 2; m = 1, -1), \tag{A7}
 \end{aligned}$$

where the parameters are written by

$$\begin{aligned}
 \Pi_1^1(k) &= -\frac{1}{\sqrt{6\pi k}} \iint dr_1 dr_2 e^{i(\sigma_1 + \delta_1)} [r_1 \tilde{R}_{k,1}(r_1)] [r_2 R_{\text{He}^+}(r_2)] \left(\frac{\partial}{\partial r_1} - \frac{1}{r_1} \right) R(r_1, r_2), \\
 \Pi_2^1(k) &= (-i)^3 \alpha \frac{1}{\sqrt{30\pi k}} \iint dr_1 dr_2 e^{i(\sigma_2 + \delta_2)} [r_1 \tilde{R}_{k,2}(r_1)] [r_2 R_{\text{He}^+}(r_2)] \left(r_1 \frac{\partial}{\partial r_1} - 1 \right) R(r_1, r_2), \\
 \Pi_{10}^1(k) &= (-i) \alpha \frac{1}{\sqrt{3\pi k}} \iint dr_1 dr_2 e^{i(\sigma_1 + \delta_1)} [r_1 \tilde{R}_{k,1}(r_1)] [r_2 R_{\text{He}^+}(r_2)] r_1 R(r_1, r_2), \\
 \Pi_1^2(k) &= -\frac{1}{\sqrt{12\pi k}} \int dr e^{i(\sigma_1 + \delta_1)} [r \tilde{R}_{k,1}(r)] \left(\frac{\partial}{\partial r} - \frac{1}{r} \right) [r R_{\text{He}^+}(r)], \\
 \Pi_2^2(k) &= (-i)^3 \alpha \frac{1}{\sqrt{60\pi k}} \int dr e^{i(\sigma_2 + \delta_2)} [r \tilde{R}_{k,2}(r)] \left(r \frac{\partial}{\partial r} - 1 \right) [r R_{\text{He}^+}(r)], \\
 \Pi_{10}^2(k) &= (-i) \alpha \frac{1}{\sqrt{6\pi k}} \int dr e^{i(\sigma_1 + \delta_1)} [r \tilde{R}_{k,1}(r)] r [r R_{\text{He}^+}(r)], \\
 F_1^x &= A_x, \quad F_1^y = A_y, \quad F_2^x = E_x, \quad F_2^y = E_y. \tag{A8}
 \end{aligned}$$

Based on these expressions, one can derive the momentum distribution of two electrons $P_{\text{model}}(\mathbf{k}_1, \mathbf{k}_2)$. As for the calculation parameters, the average radial spacing is about 0.1 a.u., and there are only 26 partial waves without free-propagation time. Other parameters are the same as TDSE calculation.

APPENDIX B: MOMENTUM TRANSFER WITH SAE APPROXIMATION

We show the results of PSI of helium based on the SAE approximation, which is briefly mentioned in Sec. III. The model potential is expressed by $V_{\text{eff}} = -\frac{1}{r} [1 + (1 + \frac{27}{16}r)e^{-\frac{27}{8}r}]$ with

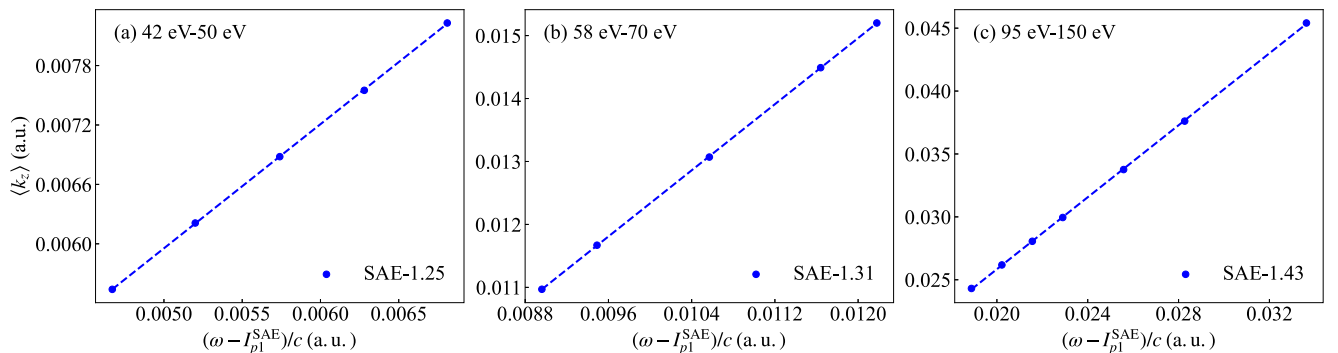


FIG. 6. The momentum transferred to the electron with SAE approximation at different photon energy regimes. The lines in each panel represent the linear fitting, and their slopes are indicated in the legends.

the ionization energy $I_{p1}^{\text{SAE}} = 24.6$ eV. The calculation is done through propagation with single-electron TDSE program with FE-DVR. We show the results of the parameter $F^{\text{SAE}} = \langle k_z \rangle / (\omega - I_{p1}^{\text{SAE}}/c)$ as a function of photon energy in Fig. 5. Clearly one finds that the nonlinear behavior also appears, which is consistent with the discussion in Sec. III. As well, we show the momentum transferred to electron at three different energy regimes in Fig. 6. In the spirit of virtual sequential

picture, these results should be compared with the fast electron of TPDI. The corresponding slopes of fast electron in these regimes of two-electron TDSE results are 1.17, 1.21, and 1.43, respectively. One finds in the energy regime from 95 to 150 eV that the slope of SAE approximation is almost the same as the fast electron in TPDI. However, the slope in the relatively slow energy regime deviates from the fast electron in TPDI.

-
- [1] H. R. Reiss, *J. Phys. B: At. Mol. Opt. Phys.* **47**, 204006 (2014).
- [2] M.-X. Wang, S.-G. Chen, H. Liang, and L.-Y. Peng, *Chin. Phys. B* **29**, 013302 (2020).
- [3] C. T. L. Smeenk, L. Arissian, B. Zhou, A. Mysyrowicz, D. M. Villeneuve, A. Staudte, and P. B. Corkum, *Phys. Rev. Lett.* **106**, 193002 (2011).
- [4] A. Ludwig, J. Maurer, B. W. Mayer, C. R. Phillips, L. Gallmann, and U. Keller, *Phys. Rev. Lett.* **113**, 243001 (2014).
- [5] J. Liu, Q. Z. Xia, J. F. Tao, and L. B. Fu, *Phys. Rev. A* **87**, 041403(R) (2013).
- [6] J. F. Tao, Q. Z. Xia, J. Cai, L. B. Fu, and J. Liu, *Phys. Rev. A* **95**, 011402(R) (2017).
- [7] A. S. Titi and G. W. F. Drake, *Phys. Rev. A* **85**, 041404(R) (2012).
- [8] S. Chelkowski, A. D. Bandrauk, and P. B. Corkum, *Phys. Rev. Lett.* **113**, 263005 (2014).
- [9] P.-L. He, D. Lao, and F. He, *Phys. Rev. Lett.* **118**, 163203 (2017).
- [10] S. Chelkowski, A. D. Bandrauk, and P. B. Corkum, *Phys. Rev. A* **95**, 053402 (2017).
- [11] S. Chelkowski and A. D. Bandrauk, *Phys. Rev. A* **97**, 053401 (2018).
- [12] A. Hartung, S. Eckart, S. Brennecke, J. Rist, D. Trabert, K. Fehre, M. Richter, H. Sann, S. Zeller, K. Henrichs *et al.*, *Nat. Phys.* **15**, 1222 (2019).
- [13] A. Sommerfeld and G. Schur, *Ann. Phys.* **396**, 409 (1930).
- [14] M. J. Seaton, *J. Phys. B: At. Mol. Opt. Phys.* **28**, 3185 (1995).
- [15] G. Massacrier, *Astron. Astrophys.* **309**, 979 (1996).
- [16] M.-X. Wang, X.-R. Xiao, H. Liang, S.-G. Chen, and L.-Y. Peng, *Phys. Rev. A* **96**, 043414 (2017).
- [17] D. Lao, P.-L. He, and F. He, *Phys. Rev. A* **93**, 063403 (2016).
- [18] H. Liang, M.-X. Wang, X.-R. Xiao, Q. Gong, and L.-Y. Peng, *Phys. Rev. A* **98**, 063413 (2018).
- [19] M. Hentschel, R. Kienberger, C. Spielmann, G. A. Reider, N. Milosevic, T. Brabec, P. Corkum, U. Heinzmann, M. Drescher, and F. Krausz, *Nature (London)* **414**, 509 (2001).
- [20] P.-M. Paul, E. S. Toma, P. Breger, G. Mullot, F. Augé, P. Balcou, H. G. Muller, and P. Agostini, *Science* **292**, 1689 (2001).
- [21] P. Emma, R. Akre, J. Arthur, R. Bionta, C. Bostedt, J. Bozek, A. Brachmann, P. Bucksbaum, R. Coffee, F.-J. Decker *et al.*, *Nat. Photonics* **4**, 641 (2010).
- [22] B. W. McNeil and N. R. Thompson, *Nat. Photonics* **4**, 814 (2010).
- [23] T. Ishikawa, H. Aoyagi, T. Asaka, Y. Asano, N. Azumi, T. Bizen, H. Ego, K. Fukami, T. Fukui, Y. Furukawa *et al.*, *Nat. Photonics* **6**, 540 (2012).
- [24] S. Grundmann, M. Kircher, I. Vela-Perez, G. Nalin, D. Trabert, N. Anders, N. Melzer, J. Rist, A. Pier, N. Strenger *et al.*, *Phys. Rev. Lett.* **124**, 233201 (2020).
- [25] S.-G. Chen, W.-C. Jiang, S. Grundmann, F. Trinter, M. S. Schöffler, T. Jahnke, R. Dörner, H. Liang, M.-X. Wang, L.-Y. Peng, and Q. Gong, *Phys. Rev. Lett.* **124**, 043201 (2020).
- [26] W.-C. Jiang, J.-Y. Shan, Q. Gong, and L.-Y. Peng, *Phys. Rev. Lett.* **115**, 153002 (2015).
- [27] J. Feist, S. Nagele, R. Pazourek, E. Persson, B. I. Schneider, L. A. Collins, and J. Burgdörfer, *Phys. Rev. Lett.* **103**, 063002 (2009).
- [28] Y.-K. Fang, H. Liang, W.-C. Jiang, and L.-Y. Peng, *Phys. Rev. A* **105**, 013104 (2022).
- [29] T. N. Rescigno and C. W. McCurdy, *Phys. Rev. A* **62**, 032706 (2000).
- [30] L. Tao, C. W. McCurdy, and T. N. Rescigno, *Phys. Rev. A* **82**, 023423 (2010).
- [31] W.-C. Jiang, W.-H. Xiong, T.-S. Zhu, L.-Y. Peng, and Q. Gong, *J. Phys. B: At. Mol. Opt. Phys.* **47**, 091001 (2014).
- [32] A. Palacios, T. N. Rescigno, and C. W. McCurdy, *Phys. Rev. Lett.* **103**, 253001 (2009).
- [33] D. A. Horner, F. Morales, T. N. Rescigno, F. Martín, and C. W. McCurdy, *Phys. Rev. A* **76**, 030701(R) (2007).
- [34] D. A. Horner, C. W. McCurdy, and T. N. Rescigno, *Phys. Rev. A* **78**, 043416 (2008).
- [35] A. Palacios, T. N. Rescigno, and C. W. McCurdy, *Phys. Rev. A* **79**, 033402 (2009).
- [36] D. A. Horner, T. N. Rescigno, and C. W. McCurdy, *Phys. Rev. A* **81**, 023410 (2010).
- [37] D. Verner, G. J. Ferland, K. Korista, and D. Yakovlev, *Astrophys. J.* **465**, 487 (1996).
- [38] J. Feist, R. Pazourek, S. Nagele, E. Persson, B. I. Schneider, L. A. Collins, and J. Burgdörfer, *J. Phys. B: At. Mol. Opt. Phys.* **42**, 134014 (2009).
- [39] T. Kato, *Commun. Pure Appl. Math.* **10**, 151 (1957).
- [40] S. Jones, J. H. Macek, and D. H. Madison, *Phys. Rev. A* **70**, 012712 (2004).
- [41] S. Bhattacharyya, A. Bhattacharyya, B. Talukdar, and N. C. Deb, *J. Phys. B: At. Mol. Opt. Phys.* **29**, L147 (1996).
- [42] K. V. Rodriguez, G. Gasaneo, and D. M. Mitnik, *J. Phys. B: At. Mol. Opt. Phys.* **40**, 3923 (2007).
- [43] O. Chuluunbaatar, I. V. Puzynin, P. S. Vinitzky, Y. V. Popov, K. A. Kouzakov, and C. Dal Cappello, *Phys. Rev. A* **74**, 014703 (2006).
- [44] A. T. Kruppa, J. Kovács, and I. Hornyak, *J. Phys. B: At. Mol. Opt. Phys.* **52**, 215001 (2019).